Theoretical illumination of highly original photoreactive ³MC states and the mechanism of the photochemistry of Ru(II) tris(bidentate) complexes

Isabelle M. Dixon,[b]* Jean-Louis Heully,[b] Fabienne Alary[b] and Paul I.P. Elliott[a]*

a Department of Chemistry, University of Huddersfield, Queensgate, Huddersfield, HD1 3DH, UK

b Laboratoire de Chimie et Physique Quantiques, UMR 5626 CNRS/Université Toulouse 3 - Paul Sabatier,

Université de Toulouse, 118 route de Narbonne, Toulouse, 31062, France

* Corresponding authors: p.i.elliott@hud.ac.uk; isabelle.dixon@irsamc.ups-tlse.fr

Abstract

We have identified highly novel photoreactive ³MC states of ruthenium(II) 4,4'-bi-1,2,3-triazolyl (btz) complexes of the form $[Ru(N^{\wedge}N)(btz)_2]^{2+}$ and have elucidated the mechanism of the highly unusual experimental observations of photochemical ligand dechelation and concomitant ligand rearrangement reactivity to form unusual photoproducts *trans*-$[Ru(N^{\wedge}N)(\kappa^2\text{-btz})(\kappa^1\text{-btz})(\text{solvent})]^{2+}$. The triplet metal-to-ligand charge-transfer (³MLCT) states and classical Jahn-Teller type triplet metal-centred (³MC) states of the series of complexes $[Ru(N^{\wedge}N)_{3-n}(btz)_n]^{2+}$ (btz = 4,4'-bi-1,2,3-triazolyl; N^N = 2,2'bipyridyl (bpy), n = 0 (**1**), 1 (**2**), 2 (**3**), 3 (**5**); N^N = 4-{pyrid-2-yl}-1,2,3-triazole (pytz), n = 1 (**4**)) have been optimised by density functional theory (DFT) and characterised. There is a gradual and significant destabilisation of the ³MLCT states as the triazole content of the complexes increases, which occurs with a slight stabilisation of the ³MC states. Whilst consistent with the promotion of photochemical reactivity in the heteroleptic complexes of the series relative to **1**, these classical ³MC states fail to account for the extraordinary ligand rearrangement processes that accompany ligand ejection. Thorough theoretical exploration of the lowest excited triplet potential energy surface (³PES) here reveals the

existence of a new type of [3]MC state and the role it plays in the photochemical reactivity of the complexes. This newly discovered state, called MC(F), displays a flattened geometry (indicated by the 'F' in the parentheses) which makes it clearly on the path to achieving the coplanarity of the bidentate ligands in the experimentally observed *trans*-photoproduct. Further novel 'pentacoodinate' [3]MC states with coplanar bidentate ligands, called MC(P) (where the 'P' in the parentheses denotes the pentacoordinate character), were then identified and optimised. The energy barriers between the different triplet states were confirmed to be small which makes all triplet states accessible. Solvent trapping, which occurs on the singlet PES according to Wigner's rules, is finally achieved by a singlet pentacoordinate species to yield the monosolvento photoproduct. Thus, our calculations not only reveal highly novel [3]MC states but more significantly demonstrate their crucial role in the formation of the experimentally observed photoproducts.

Introduction

The photophysics and photochemistry of oligopyridyl complexes of kinetically inert d^6 metals has been the subject of intense investigation over the past four decades.[1, 2] Of renewed interest in systems of this type is the interplay between the initial photoexcited metal-to-ligand-charge transfer (MLCT) states responsible for their characteristic singlet absorption ([1]MLCT) and luminescent triplet emission[3-5] ([3]MLCT) and their triplet metal-centred ([3]MC) states[6-17] that are responsible for deactivating said emission by nonradiative quenching. These [3]MC states can also be intimately involved in photochromic rearrangement and ligand dissociation reactions,[18-41] a subject that we are particularly interested in.

As an example of a typical luminescent complex the occupied frontier orbitals of $[Ru(bpy)_3]^{2+}$-type complexes[42] are predominantly metal-based while the LUMO is bpy π^* in character with the LUMO+1 and LUMO+2 orbitals having $d\pi$-bpyπ^* character. Thus the lowest energy features of the optical absorption spectra of these complexes are typically of [1]MLCT character through promotion of an electron from these metal-based orbitals to an unoccupied ligand dominated orbital (process *a* in Figure 1a and 1b). Rapid intersystem crossing due to the presence of the heavy metal centre results in efficient conversion to the triplet [3]MLCT state (process *b*). It is then radiative decay from the [3]MLCT state that leads to the characteristic phosphorescent emission

2

(process *c*). Being in close proximity, ^{3}MC states can be thermally populated from the ^{3}MLCT state (process *d*), resulting in quenching of emission and even photochemical reactivity through the weakening and elongation of metal-ligand bonds. This can therefore result in isomerisation or ligand loss reactions.

These excited states and transitions between them are often depicted using a Jablonski diagram (Figure 1a) familiar from undergraduate lectures. However, the traditional Jablonski diagram is often inadequate to satisfactorily convey the true energetics of the processes occurring as it disregards the structural distortions between ground and excited states. Indeed the ^{3}MC states are depicted as being higher in energy than the ^{3}MLCT states in a traditional Jablonski diagram (i.e. the ^{3}MC state at the ^{3}MLCT geometry), however geometry relaxation through Ru-N bond elongation can lead to the relaxed ^{3}MC state being at *lower* energy than the relaxed ^{3}MLCT state.[6, 42-44] Instead, potential energy curve descriptions (Figure 1b) are more intuitively informative. Here the reaction coordinate (r.c.) may be defined by the Ru-N bond lengths for example, and thus takes into account geometrical rearrangement after excitation. Over the last few years theoretical work has illuminated what can now be considered *classical* ^{3}MC states in which the population of a dσ* orbital leads to a Jahn-Teller type distortion in which two mutually *trans* Ru-N bonds become elongated to yield a [Ru(κ^2-N^N)(κ^1-N^N)$_2$]$^{2+}$-like structure. The efficiency of ^{3}MC population is determined by the magnitude of the activation barrier following the ^{3}MLCT $\rightarrow$ ^{3}MC minimum energy path (MEP), as well as by the overall topology of the ^{3}PES and the vibrational energy within the system.
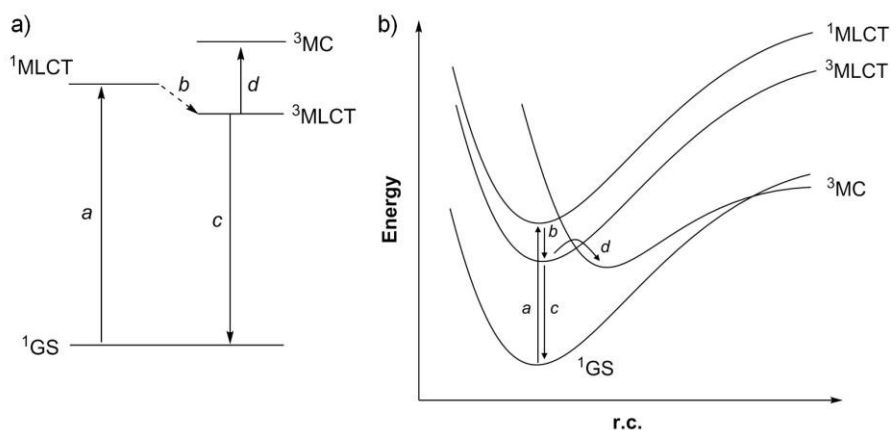

Figure 1. Jablonski (a) and qualitative potential energy curve (b) diagrams for ground and excited states for [Ru(bpy)$_3$]$^{2+}$.
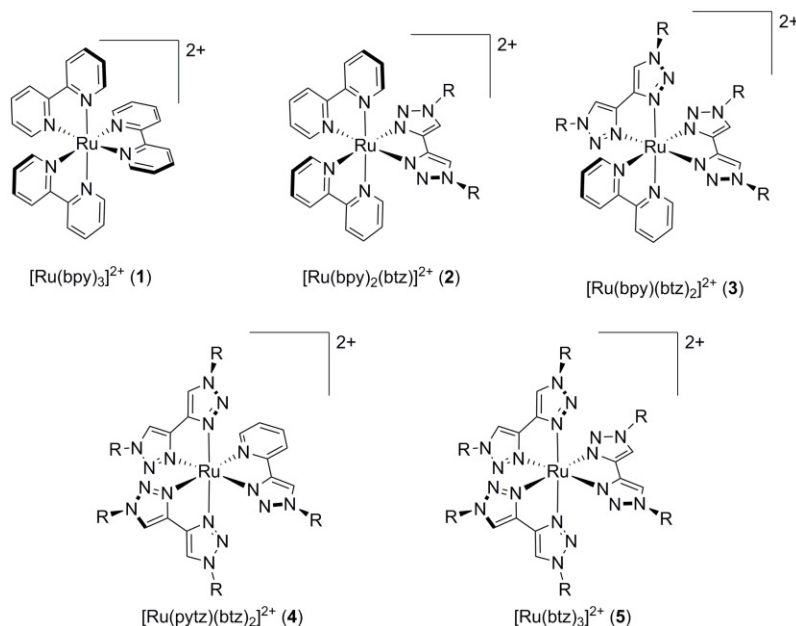
3

Chart 1. Structures of the complexes computationally investigated in this study (in our experimental studies R = benzyl, but to limit computational expense in the calculations R is simplified to methyl).

Complexes of 1,2,3-triazole-based ligands[45, 46] have revealed an extraordinary diversity in photophysical and photochemical properties, ranging from highly tunable phosphors[47-54] for light-emitting devices to efficient sensitisers for dye solar cell applications.[55] We have demonstrated that the inclusion of bitriazolyl (btz) ligands[56-59] leads to photochemical ejection of btz for ruthenium(II) complexes,[60-64] and far more extraordinarily, for osmium(II) which one would expect to be photochemically inert.[65] In the series of complexes [Ru(bpy)$_{3-n}$(btz)$_n$]$^{2+}$ (n = 0, **1**; n = 1, **2**; n = 2, **3**; n = 3, **5**; Chart 1)[66] and the pyridyltriazole (pytz) analogue **4**, [Ru(pytz)(btz)$_2$]$^{2+}$ (**4**),[60] absorption bands are observed to progressively blue-shift from **1** to **3** as the bpy-centred LUMO becomes destabilised. The absorption profile then undergoes a dramatic blue-shift for **4** and then **5,** reflecting the much higher energies of the LUMO of the pytz and btz ligands relative to that of bpy. Time-dependent DFT (TD-DFT) calculations at the ground state geometry reproduce this experimental data and confirm the bpy-localisation of the S$_1$ ^{1}MLCT states for **2** and **3**. It is noteworthy that the nature of the S$_1$ state switches from ^{1}MLCT to ^{1}MC in character for complex **5**. Thus the destabilisation of the LUMO occurs to such

an extent in this complex that the ordering of the lowest energy excited states is reversed. When optimised the lowest lying triplet states of **4** and **5** are indeed of MC nature and adopt a classical $[Ru(\kappa^2\text{-}N^\wedge N)(\kappa^1\text{-}btz)_2]^{2+}$ structure ($N^\wedge N$ = pytz and btz respectively) in which two *trans* Ru-N bonds elongate by ca. 0.4 Å.

We have recently reported the photochemical ligand ejection reactivity of **2**, **3** and **4** with efficient conversion to the bis-solvento complexes and liberation of an equivalent of free btz (Scheme 1).[60-63] This is consistent with the destabilisation of the ^{3}MLCT state reducing the activation barrier to population of the ^{3}MC state with respect to that for **1**. In the case of **2** *cis* stereochemistry in the product *cis*-$[Ru(bpy)_2(NCMe)_2]^{2+}$ (**6**) is observed, as for **1**. On the contrary, for the bis(bitriazolyl) complexes **3** and **4,** ejection of btz remarkably leads to *trans* bis(solvento) products *trans*-$[Ru(N^\wedge N)(btz)(NCMe)_2]^{2+}$ (**9** and **10**) and proceeds with the observation of ligand-loss mono(solvento) products *trans*-$[Ru(N^\wedge N)(\kappa^2\text{-}btz)(\kappa^1\text{-}btz)(NCMe)]^{2+}$ (**7** and **8**) (Scheme 1).
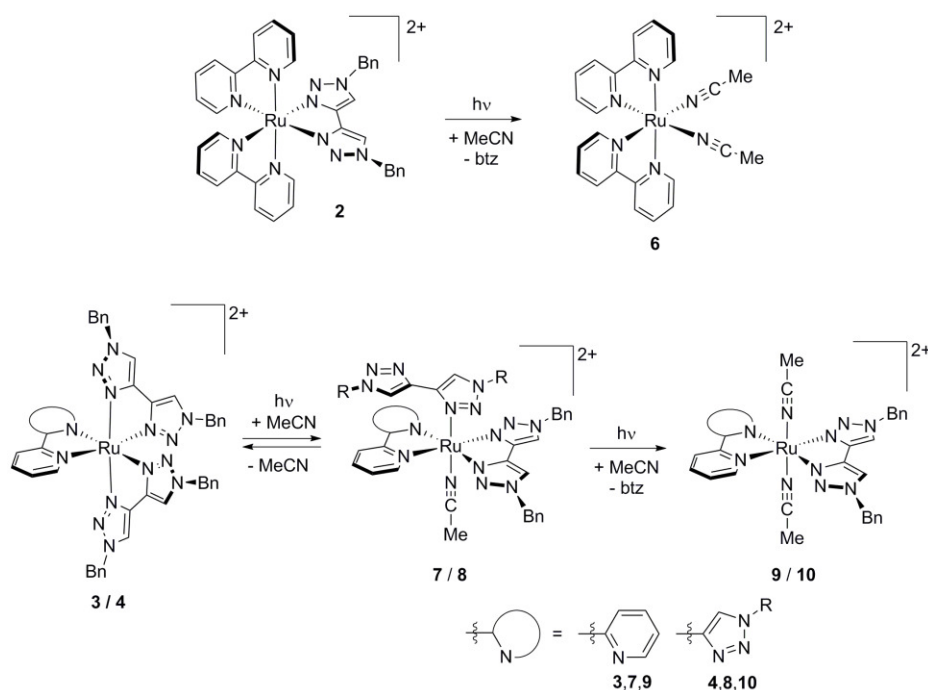
Scheme 1. Photochemical reactivity of **2**, **3** and **4** in acetonitrile solutions.[60, 62, 63]

It is noteworthy that the key actors involved in the mechanism for ligand photorelease from ruthenium complexes have been studied theoretically with *monodentate* departing ligands only, using a combination of unrestricted DFT and TD-DFT.[29, 30, 32, 33, 67-71] This reaction proceeds along a rather intuitive reaction coordinate,

i.e. Ru–L elongation, which can be probed by relaxed surface scans.[29, 30, 32, 33, 69] Mechanistic studies have emphasized the complexity and the multistep nature of ligand photolabilisation processes.[30, 67, 70, 71] However, following an in-depth study of the ^{3}PES, we have identified new structural isomers of the ^{3}MC state and have shown that, in addition to bond elongation, the reaction may also involve an offset of the departing ligand from its initial coordination axis.[70]

Despite the tremendous importance of Ru(II) complexes in sensing, solar cells or PDT to name a few of their applications, relatively little is known regarding the triplet excited state dynamic processes that result in desired (photorelease) or undesired (photoinstability) photolabilisation of bidentate ligands from Ru(II) complexes. Therefore it is still a real challenge to establish the mechanism of bidentate ligand photorelease from Ru(II) complexes.

The aim of this work was to study the mechanism of such photorelease processes by theoretical approaches. In this contribution we report theoretical characterisation of ^{3}MC states of these complexes, with a particular emphasis on those relevant to photochemical reactivity for **3** and **4**. The topology of their ^{3}PES was initially probed by series of relaxed surface scans. In addition to characterisation of *classical* $[Ru(\kappa^2\text{-}N^\wedge N)(\kappa^1\text{-}N^\wedge N)_2]^{2+}$-type ^{3}MC states, these scans have led us to identify a new type of ^{3}MC state in which two Ru-N bonds to the same btz ligand are elongated whilst the N-Ru-N angle for the Ru-N bonds *trans* to the 'distal' btz ligand undergoes significant enlargement, thus flattening the $Ru(\kappa^2\text{-}N^\wedge N)(\kappa^2\text{-}btz)$ fragment towards coplanarity (where N^N is bpy or pytz). To probe this hypothesis, we have then accentuated the flattened geometries, which were optimized to yield pseudo-pentacoordinate square pyramidal ^{3}MC local minima for complexes **3** and **4**. These states, which display coplanar bidentate ligands as observed in the photoproducts, have low energy singlet/triplet minimum energy crossing points enabling access to a square-pyramidal pentacoordinate singlet ground state with a solvent accessible coordination site. Through the use of Nudged Elastic Band calculations, we then show that this new flattened ^{3}MC state is readily accessible on the ^{3}PES with a small activation barrier to conversion from the ^{3}MLCT state. Solvent capture should be facilitated by a coordinatively unsaturated complex. We therefore not only identify highly novel and as yet unrecognised class of ^{3}MC states, but also elucidate the mechanism of the experimentally observed *trans* photochemistry for these complexes, accounting for the highly

6

unusual novel concomitant rearrangement occurring during these photodechelation reactions in coordinating solvents.

Results & Discussion

^{3}MLCT and 'classical' ^{3}MC minima

The optimised geometries of the lowest ^{3}MLCT states for complexes **1** to **3** (**1 ^{3}MLCT** to **3 ^{3}MLCT**) were calculated starting from their optimised ground states and specifying a spin multiplicity of 3. In agreement with the observed blue-shift in the ^{1}MLCT band in their UV-visible absorption spectra, the ^{3}MLCT states **1 ^{3}MLCT** to **3 ^{3}MLCT** are destabilised by approximately 0.1 eV for each replacement of bpy by btz (Figure 2). Plots of the spin density for **2 ^{3}MLCT** and **3 ^{3}MLCT** confirm the localisation of the photoexcited electron on the bpy ligands (Figure S1). As was stated on our original report[66] the optimised T$_1$ state of **5** is found to have metal-centred character. A ^{3}MLCT state, **5 ^{3}MLCT**-D$_3$, was optimised by imposing D_3 symmetry, which does not apply to the MC excited state. On incorporation of a third btz ligand the **5 ^{3}MLCT**-D$_3$ state is destabilised by 0.95 eV relative to **3 ^{3}MLCT**, reflecting the much higher energy of the btz LUMO relative to that of bpy, and lies 3.45 eV above the ground state. The calculated energies of **5 ^{3}MC** and **5 ^{3}MLCT**-D$_3$ clearly show that there will be a large energy separation between both triplet states.
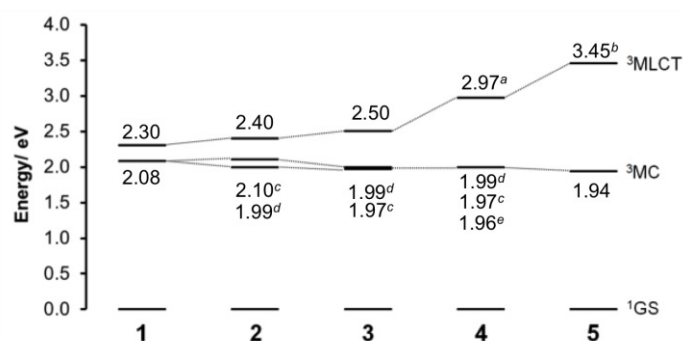

Figure 2. Plot of relative energies of the ^{3}MLCT and ^{3}MC states for complexes **1** to **4** at their respective optimised geometries relative to that of each ground state (E(^{1}GS) = 0). *a* Energy of T$_1$ state from TDDFT; *b* constrained to D_3 symmetry; *c* ^{3}MC(A); *d* ^{3}MC(B); *e* ^{3}MC(C).

7

For the pyridyltriazole complex **4** the optimisation of the T_1 state yields a ^{3}MC state.[60] A TDDFT calculation at the ground state geometry, however, indicated a T_1 state of ^{3}MLCT character. This state, **4 ^{3}MLCT**, was determined by TDDFT to lie 2.97 eV above the ground state and is intermediate in energy between **3 ^{3}MLCT** and **5 ^{3}MLCT**-D_3.

For complexes **1** to **3** ^{3}MC state geometries were calculated (see Figure 3) through optimisations starting from initial estimate geometries; firstly, the localisation of the d_z^2-like and $d_{x^2-y^2}^2$-like antibonding dσ* orbitals for the ground states were examined to identify the participating Ru-N bonds (see Figure S2). For each complex, a pair of initial estimate geometries were then prepared by elongation of the principal participating Ru-N bonds to 2.4-2.5 Å. These geometries were then allowed to optimise with a spin multiplicity of 3. In every case, classical $[Ru(\kappa^2\text{-}N^\wedge N)(\kappa^1\text{-}N^\wedge N)_2]^{2+}$ type geometries are obtained with two mutually *trans* elongated Ru-N bonds. Selected structural parameters are reported on Figure 3 and in Table S1. Mulliken spin densities for these ^{3}MC states were also plotted and are presented in Figure S3.

For **1** both initial estimate geometries resulted in isostructural ^{3}MC states with elongated Ru-N bond lengths of 2.46 Å, reproducing our previously reported calculated structures for this complex and similar to that found for $[Ru(bpz)_3]^{2+}$ (bpz = 2,2'-bipyrazine).[42, 43] In addition to bond elongation, the ^{3}MC state of **1** displays a significant rotation of the decoordinated pyridine ring relative to the coordinated ring with a N-C-C-N dihedral angle of 13.2 ° (Table S1).

In the cases of the heteroleptic complexes **2** and **3**, this resulted in a pair of ^{3}MC states for each; one of these ^{3}MC states is approximately C_2 symmetric (termed ^{3}MC(A) in each case: **2 ^{3}MC(A)** and **3 ^{3}MC(A)**) involving dechelation of both bpy ligands in the case of **2** and both btz ligands in the case of **3**. A similar elongated Ru-N bond distance and twist in the κ^1-bpy ligands to that observed for **1 ^{3}MC** is found for **2 ^{3}MC(A)** (2.46 Å and 10.9 °). This elongation occurs to a greater extent in **3 ^{3}MC(A)** with elongated Ru-N lengths of 2.54 Å (near identical to **5 ^{3}MC**) but a much smaller N-C-C-N dihedral angle of 0.3 °.

The other, asymmetric, ^{3}MC(B) states for **2** and **3** (**2 ^{3}MC(B)** and **3 ^{3}MC(B)**) respectively) involve dechelation of one bpy and one btz ligand. For both **2 ^{3}MC(B)** and **3 ^{3}MC(B)** the lengthened Ru-N(bpy) bond is shorter than found for **1 ^{3}MC** or **2 ^{3}MC(A)** at 2.38 Å, whilst the Ru-N(btz) bond length is significantly longer than in **3 ^{3}MC(A)** at 2.71 Å. These structural effects are likely to partly stem from the greater π-acceptor character of the pyridine moieties over triazole, which will result in a larger *trans* effect for the former.
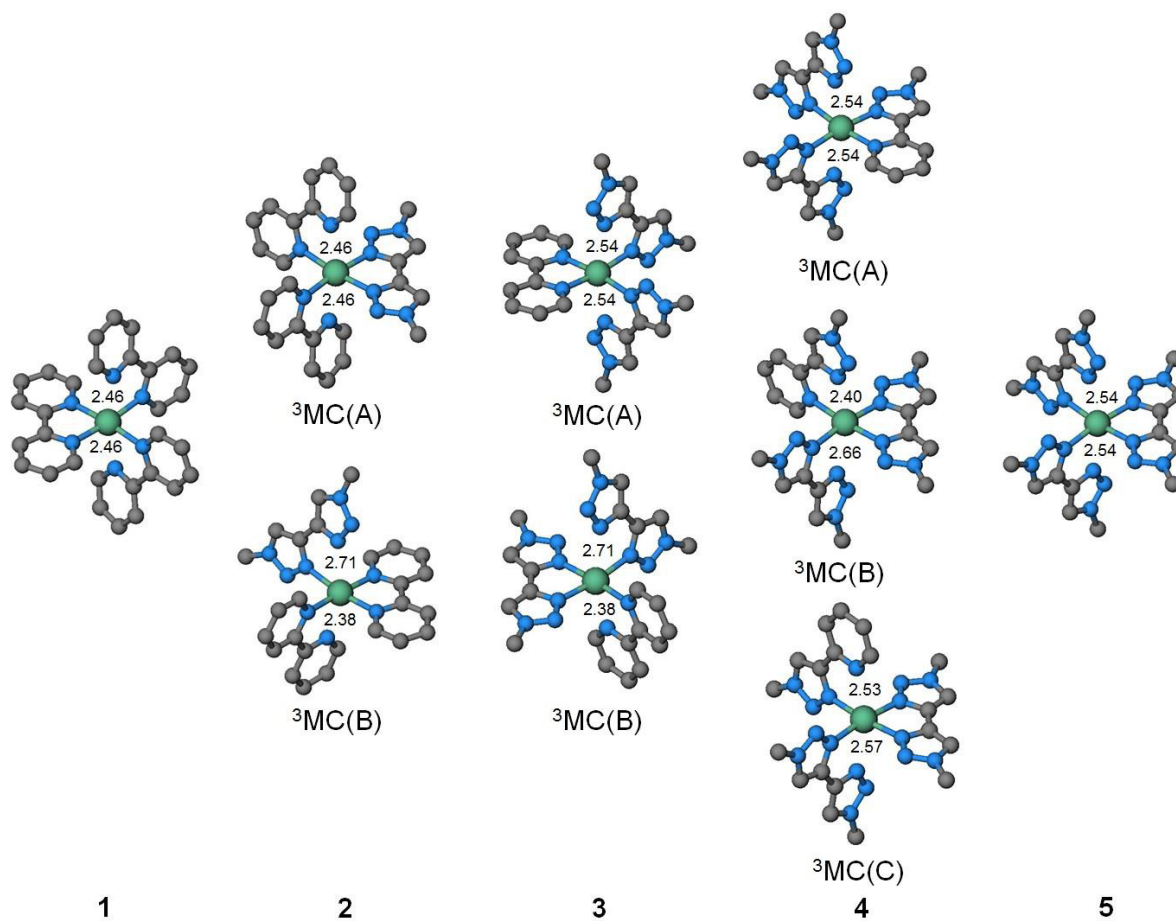

Figure 3. Structures of the optimised geometries of classical ^{3}MC states for complexes **1** to **5** annotated with distances for elongated Ru-N bonds (hydrogen atoms omitted for clarity).

For **3**, the ^{3}MC(A) and ^{3}MC(B) pair is nearly isoenergetic (Figure 2). Across the series there is a general destabilisation of the ^{3}MLCT states and stabilisation of the ^{3}MC states from approximately 2.1 eV for **1** and **2** to 1.94 eV for **5**. Increasing btz content induces a concomitant destabilisation of the ^{3}MLCT states and stabilisation

of the ^{3}MC states. Whilst this does not tell us explicitly about the magnitude of the barriers to excited state conversion this is consistent with the experimentally observed increasing photoreactivity from **1** to **3**.

Optimisation of the lowest triplet excited states of **4** (**4 ^{3}MC(A)**) and **5** (**5 ^{3}MC**) result in ^{3}MC states with the classical structure *trans*-[Ru(κ^2-N^N)(κ^1-btz)$_2$]$^{2+}$ (N^N = pytz or btz, Figure 3). The asymmetry of the pytz ligand in **4** renders each of the three N-Ru-N axes unique, enabling two further classical ^{3}MC states in addition to **4 ^{3}MC(A)** to be envisaged. Initial guess geometries were therefore prepared elongating Ru-N bonds along the N(py*tz*)-Ru-N and N(*py*tz)-Ru-N axes which were then allowed to optimise. The resultant ^{3}MC states, **4 ^{3}MC(B)** and **4 ^{3}MC(C)** respectively, are very close in energy to that of **4 ^{3}MC(A)**.

Relaxed ^{3}PES scans leading to new flattened ^{3}MC states

For these complexes, optimisation of ^{3}MC minima in itself does not provide any significant mechanistic insight into the photochemical reactivity of the complexes described, but does give a clear view of the complexity of the ^{3}PES. In particular, classical ^{3}MC states fail to account for the observed rearrangements in the photochemistry of **3** and **4,** in which the remaining bidentate ligands become coplanar. Therefore, to gain a deeper understanding of the excited state dynamics in these photochemically reactive systems, we turned our attention to probing the topology of the ^{3}PES connecting the ^{3}MLCT and ^{3}MC states. We initially conducted relaxed ^{3}PES scans starting from the ^{3}MLCT geometries in an attempt to map the landscape of the triplet manifold and obtain an indication of the magnitude of energy barriers for ^{3}MC state population.

For complexes **2** and **3**, where the T_1 state has ^{3}MLCT character at the ground state geometry, relaxed ^{3}PES scans were carried out through Ru-N bond elongations starting from the optimised ^{3}MLCT geometries. For complex **4**, where previous calculations had indicated that the T_1 state is of ^{3}MC character,[60] relaxed ^{3}PES scans were conducted in which the elongated bond distances in **4 ^{3}MC(A)**, **4 ^{3}MC(B)** and **4 ^{3}MC(C)** were contracted in anticipation that this might lead to a ^{3}MLCT state, or more likely, to a transition between the different ^{3}MC states as previously observed in ^{3}PES scans for cyclometalated iridium complexes.[72]

In the case of **2**, relaxed ^{3}PES scans involving elongation of one of the Ru-N(bpy) ligands *cis* to btz and one of the Ru-N(btz) bonds leads to formation of the expected geometries for **2 ^{3}MC(A)** and **2 ^{3}MC(B)** respectively with energy barriers of ~0.04 to 0.05 eV (1 kcal mol^{-1}) (Figure S4). For complex **3**, whilst elongation of one of the Ru-N(btz) bonds *trans* to bpy yields the expected **3 ^{3}MC(B)** state (Figure S5), it is highly noteworthy that the ^{3}PES scan involving elongation of one of the mutually *trans* Ru-N(btz) bonds fails to arrive at **3 ^{3}MC(A)** but instead yields an entirely new ^{3}MC state (Figure 4a, blue energy profile); as bond *a* as defined in Figure 4a undergoes elongation, bonds *b* and *c* are observed to elongate temporarily, forming a distorted **3 ^{3}MC(B)**-like geometry before bond *c* contracts leaving bond *b* extended. Concomitantly the angle between bonds *c* and *d* is observed to widen, thus generating a new flattened ^{3}MC state geometry (**3 ^{3}MC(F)** where the "F" denotes the flattened nature of the [Ru(κ^2-bpy)(κ^2-btz)] moiety) with a single *distal* btz ligand in which *both* Ru-N bonds are extended. The same state is arrived at for a ^{3}PES scan conducted contracting Ru-N bond distance *d* starting from the optimised geometry for **3 ^{3}MC(A)**, whereby bond *b* is induced to elongate as the angle between bonds *d* and *c* widens (Figure 4a, red energy profile). The geometry of **3 ^{3}MC(F)** was allowed to optimise free of geometric constraints and converged to a true minimum (Figure 5 middle), whose key parameters are summarised in Table 3. These data suggest that depopulation of the ^{3}MLCT state and population of the ^{3}MC states is irreversible and that the three ^{3}MC states (**A**, **B** and **F**-type) are connected to one another. Similar behaviour was observed by Zhou *et al.* in their ^{3}PES scans in triscyclometalated iridium(III) complexes.[72] After population the ^{3}MC states may then either undergo direct deactivation to the ground state, or may go on to yield the observed κ^1-btz photochemical reaction product.
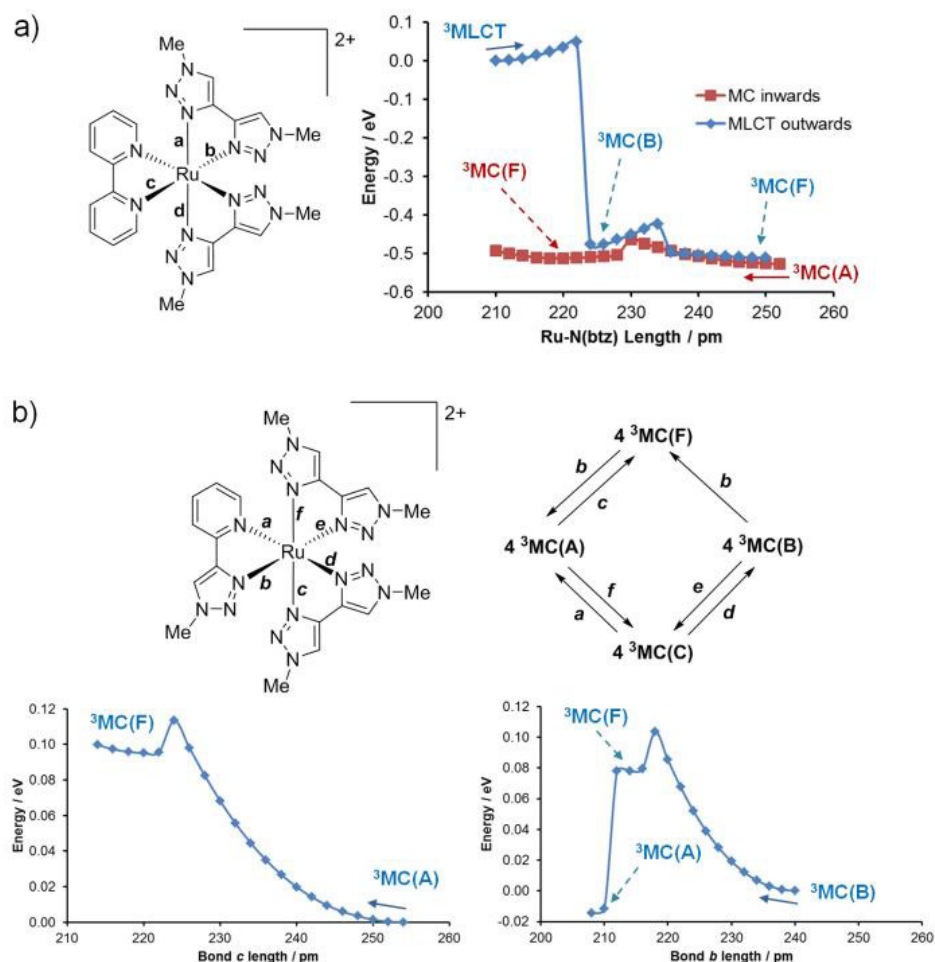
Figure 4. a) Relaxed ^{3}PES scans for **3 ^{3}MLCT** $\rightarrow$ **3 ^{3}MC(F)** and **3 ^{3}MC(A)** $\rightarrow$ **3 ^{3}MC(F)**, b) Summarised ^{3}MC interconversion during ^{3}PES scans for ^{3}MC states of **4** with energy profile plots for **4 ^{3}MC(A)** $\rightarrow$ **4 ^{3}MC(F)** and **4 ^{3}MC(B)** $\rightarrow$ **4 ^{3}MC(F)** scans (Note: the x-axis distances refer to the Ru-N distance undergoing elongation or contraction in each case).

For complex **4**, a series of relaxed ^{3}PES scans were carried out for contraction of the extended Ru-N bonds a through f starting from each of the respective classical ^{3}MC state geometries (Figure S6). Figure 4b summarises the interconversions that are observed to occur during these calculations. Crucially we observe that contraction of bond c starting from **4 ^{3}MC(A)** and bond b starting from **4 ^{3}MC(B)** both lead to an analogous flattened ^{3}MC state, **4 ^{3}MC(F)**, whose geometry was then optimised to a true minimum on the basis of these scans without geometric constraints (Figure 5 right and Table S2).

12

Whilst no such state is observed in the course of the ^{3}PES scans for **2** (Figure S4) we utilised the geometric parameters for **3 ^{3}MC(F)** and **4 ^{3}MC(F)** in order to derive a suitable estimate geometry for optimisation of the analogous state **2 ^{3}MC(F)**, which we were indeed able to locate (Figure 5 left and Table S2). Attempts were made to locate a similar state for **5** but without success with optimisations resulting in a classical **5 ^{3}MC** geometry.

Geometric and electronic structure of the new flattened ^{3}MC states

The extended Ru-N bonds to the *distal* btz ligands vary from 2.39 to 2.53 Å in the three ^{3}MC(F) states with N-Ru-N angles θ (between the Ru-N bonds that were *trans* to the now *distal* btz ligand) ranging from 124.5 ° for **2 ^{3}MC(F)** to 136.1 ° for **3 ^{3}MC(F)** (Figure 5 and Table S2). For each ^{3}MC(F) state, plots of the spin density demonstrate that the unpaired electrons are primarily localised on the metal centre thereby confirming their ^{3}MC character (Figure S3).
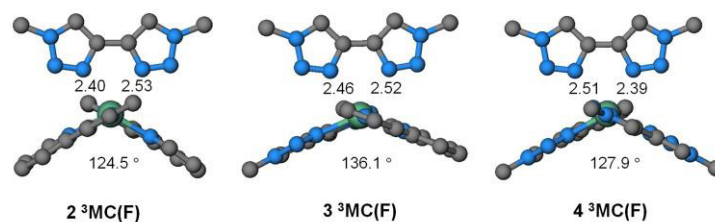

2.40 2.53   2.46 2.52   2.51 2.39

124.5 °   136.1 °   127.9 °

2 ^{3}MC(F)   **3 ^{3}MC(F)**   **4 ^{3}MC(F)**

Figure 5. Optimised geometries of ^{3}MC(F) states of **2**, **3** and **4** with annotated elongated Ru-N distances (Å) and widened angle θ between Ru-N bonds *trans* to elongated Ru-N bonds (hydrogen atoms omitted for clarity).

The observation in our calculations of these ^{3}MC(F)-type flattened states demands explanation. In 'classical' ^{3}MC states, population of a "d_z^2-like" $d\sigma^*$ orbital results in a double Ru–N bond elongation. It is possible to derive classical-type ^{3}MC states with elongation along each of the three possible N-Ru-N axes (e.g. as in the case of **4**). Besides, formal population of a "$d_{x^2-y^2}$-like" $d\sigma^*$ orbital is also possible, with distortion

13

involving all three ligands. Elongation of both Ru-N bonds of one chelate ligand, both of whose N-atoms participate in the dσ* orbital, will diminish metal-ligand orbital overlap thus stabilising this state. Additionally, concomitant deviation from linearity of orbital overlap of the two N atoms *trans* to the elongated Ru-N bonds, by flattening of the Ru(N^N)$_2$-fragment towards coplanarity with enlargement of the angle θ, will further stabilise the dσ* orbital. Thus, the MC(F) states are nearly degenerate with the classical MC states. The MC(F) states calculated here (**2 ^{3}MC(F)**, **3 ^{3}MC(F)** and **4 ^{3}MC(F)**, Figure 5) represent a novel class of ^{3}MC states additional to the 'classical' ^{3}MC states described. Since **4** exhibits the broadest range of ^{3}MC states Figure 6 shows the pairs of singly occupied natural orbitals of **4 ^{3}MC(A-C)** and **4 ^{4}MC(F)**, which illustrate the "d_z^2-like" vs "$d_{x^2-y^2}$-like" origin of their structural distortions. They are representative of all ^{3}MC states discussed in this work. For each of the classical states **4 ^{3}MC(A-C)** the SONO+1 is of predominantly d_z^2-like dσ*-orbital character with alignment along the elongated N-Ru-N axis. In contrast that of **4 ^{4}MC(F)** clearly exhibits $d_{x^2-y^2}$-like dσ* character.

4 ^{3}MC(A)   **4 ^{3}MC(B)**   **4 ^{3}MC(C)**   **4 ^{3}MC(F)**
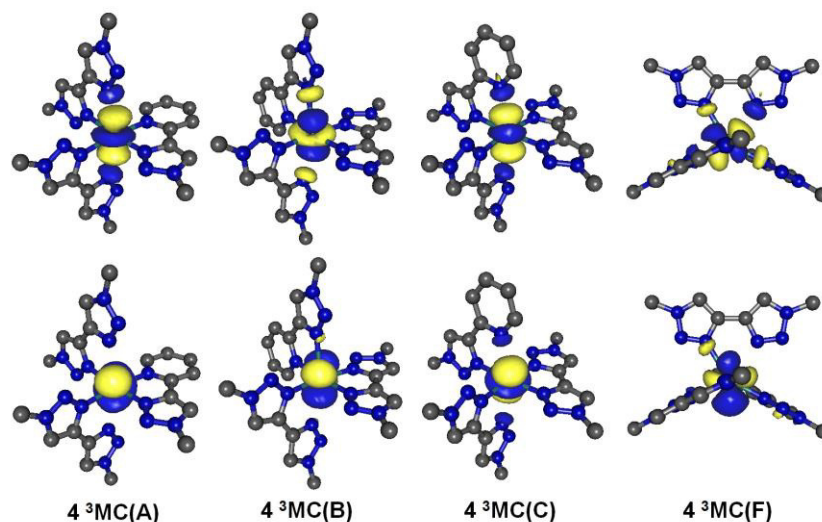
Figure 6. Singly occupied natural orbitals (SONO (bottom)/SONO+1 (top)) of **4 ^{3}MC(A-C)** and **4 ^{3}MC(F)** (hydrogen atoms omitted for clarity).

Flattening of the M(L^L)$_2$ fragment where the ligands in the ground state are approximately orthogonal has been characterised in calculations on trigonal bipyramidal formally pentacoordinate ^{3}MC states, for example,

for triscyclometalated iridium(III) complex ^{3}MC states of the type [Ir(κ^2-C^N)$_2$(κ^1-C^N)] where the κ^1-C^N ligand is indeed monodentate and dechelated with a large dihedral angle between the planes of the two rings of the dechelated ligand.[73] Flattening has also been observed in calculations on pentacoordinate ruthenium(II) species[67] but examples of this behaviour in "hexacoordinate" ^{3}MC states are almost unknown. This type of flattening has been observed previously in ruthenium(II) ^{3}MC state calculations but its full significance perhaps not recognised at the time; in calculations on the S/O-donor linkage photoisomerisation of [Ru(bpy)$_2$(O^S)]$^+$ (where O^S is a 2-carboxyphenylsulphoxide ligand) to [Ru(bpy)$_2$(O^O')]$^+$, Göttle *et al.* noted a flattening of the Ru(bpy)$_2$-fragment in one of the key ^{3}MC states involved in the isomerisation mechanism.[20]

In our experimental photochemistry only ejection of the btz ligands is observed, which clearly indicates the need for participating ^{3}MC states to involve elongation of Ru-N bonds to the departing btz ligand. This prompted us, however, to investigate whether an analogous flattened ^{3}MC state could be found for **3** in which the distal ligand is now bpy. After several attempts such a geometry was optimised (**3 ^{3}MC(F)'**, Figure S7) and lies some 0.3 eV higher in energy than **3 ^{3}MC(F)** and is therefore unlikely to be populated. We attribute this destabilisation to the greater π-acceptor character of the bpy ligand over btz, which reduces the propensity for the elongation of Ru-N(bpy) bonds (c.f. the significantly shorter Ru-N(bpy) distances compared to the Ru-N(btz) distances in the geometries of **2 ^{3}MC(B)** and **3 ^{3}MC(B)**, Figure 3). With regards to the mechanism of photochemical ejection that is experimentally observed for the btz ligands detailed here, ^{3}MC(F)'-type states with a distal bpy or pytz ligand are thus discounted in our discussion. We should also note that an alternative ^{3}MC(F)-type state can be envisage in the case of **4** in which the btz lying *trans* rather than *cis* to the pyridine ring of the pytz ligand adopts the distal position. Since this alternative state is not seen in our ^{3}PES scan studies described earlier this is also discounted from further discussion.

Nonradiative deactivation of classical and flattened ^{3}MC states via singlet-triplet ISC

To probe the propensity of the complexes for nonradiative deactivation, we then optimised the singlet-triplet minimum energy crossing points (^{1,3}MECPs)[74, 75] for all classical and new flattened ^{3}MC states of the photoreactive complexes **2**, **3** and **4** (Table 1). Singlet state geometry optimisations starting from the ^{1,3}MECP

geometries for the classical ^{3}MC states for these complexes results in the full recoordination of the ligands and relaxation to the initial ground state geometry in each case. Therefore, MECPs(A/B/C) bring the system back to its initial reactant state.

The ^{1,3}MECP for **3 ^{3}MC(F)** (**3 ^{1,3}MECP(F)**) resides 0.13 eV higher in energy than the minimum for this state. At the **3 ^{1,3}MECP(F)** geometry one of the Ru-N distances to the distal btz ligand shortens to 2.35 Å whilst the other further elongates to 2.67 Å, indicating that this btz ligand is on the path to becoming formally monodentate. However, when a singlet state is optimised starting from **3^{1,3}MECP(F)** the complex reverts to the fully hexacoordinate pseudo-octahedral reactant ground state. Optimisation of the singlet state from the analogous **4 ^{1,3}MECP(F)** geometry similarly yields the ground state of **4**. Thus **3/4 ^{1,3}MECP(F)** can be seen as quenchers of photochemistry rather than as a route to the observed photoproducts. However, since the Ru(N^N)(κ^2-btz) fragments in **3 ^{3}MC(F)** and **4 ^{3}MC(F)** would appear to be approximately half way to the coplanarity in the photoproducts **7** and **8**, rather than representing the final stages on the ^{3}PES en route to the photoproducts, these states are clearly possible intermediate ^{3}MC states to further ^{3}MC states responsible for formal coplanarisation.

Table 1. Energies (eV) of ^{1,3}MECPs for ^{3}MC states of **2**, **3** and **4** quoted relative to minimum of ^{3}MC state in question. **A/B/C** stand for d_{z^2}-type 'classical' ^{3}MC states; **F** stands for new $d_{x^2-y^2}$-type flattened ^{3}MC states; **P** stands for pseudo-pentacoordinate.

2 ^{3}MECP(A)	0.28	3 ^{3}MECP(A)	0.16	4 ^{3}MECP(A)	0.16
2 ^{3}MECP(B)	0.15	3 ^{3}MECP(B)	0.18	4 ^{3}MECP(B)	0.21
2 ^{3}MECP(F)	0.05	3 ^{3}MECP(F)	0.13	4 ^{3}MECP(C)	0.21
		3 ^{3}MECP(P)	0.05	4 ^{3}MECP(F)	0.16
				4 ^{3}MECP(P)	0.09

Pseudo-pentacoordinate triplet and pentacoordinate singlet states

16

Following this line of reasoning, initial guess geometries for further ^{3}MC states were derived from those of **3 ^{3}MC(F)** and **4 ^{3}MC(F)** in which the Ru(N^N)(κ^2-btz) fragments were set to be approximately co-planar, as in the primary photoproducts. For both **3 ^{3}MC(F)** and **4 ^{3}MC(F)** the N donor atoms of the triazole ring of the distal btz ligand with the shortest Ru-N distance was positioned in the approximate square pyramidal axial position. Triplet state optimisation then allowed us to obtain the geometries of two new ^{3}MC minima **3 ^{3}MC(P)** and **4 ^{3}MC(P)** (where the "P" denotes the pseudo-pentacoordinate nature of these states, Figure 7 and Table S2). The distal btz in **3 ^{3}MC(P)** and **4 ^{3}MC(P)** maintain approximately coplanar triazole rings and have Ru-N distances of 2.44 and 3.20 Å for **3 ^{3}MC(P)** whereas those in **4 ^{3}MC(P)** are 2.51 and 2.77 Å. **3 ^{3}MC(P)** lies only 0.05 eV (1 kcal mol^{-1}) above **3 ^{3}MC(F)** (and thus these states are effectively degenerate) whereas **4 ^{3}MC(P)** lies 0.14 eV (3 kcal mol^{-1}) above **4 ^{3}MC(F)**.

Geometries for the ^{1,3}MECPs associated with **3 ^{3}MC(P)** and **4 ^{3}MC(P)**, i.e. **3 MECP(P)** and **4 MECP(P)**, were optimised and are located 0.05 and 0.09 eV higher in energy than their respective ^{3}MC state minima (Figure 7). These highly accessible MECPs are the connection between the reactive ^{3}PES and a singlet PES suitable for Wigner-allowed solvent trapping. Strikingly, singlet state geometry optimisation starting at these ^{1,3}MECP(P)s yields formally pentacoordinate, distorted square pyramidal species **3 ^{1}GS(P)** and **4 ^{1}GS(P)** (Figure 7 and Table S2), which are the missing link to the photoproducts and were hypothesized in previous work.[70] In each case the distal btz ligand now adopts a formally monodentate coordination mode with a Ru-N bond length of approximate 2.05 Å and exhibits a significant torsion angle between the planes of the two triazole rings. Although initially discussed in the context of excitation into MC states, the importance of MECP(P) was already highlighted in 1983, as formulated by Vanquickenborne and Ceulemans for d^6 complexes: '*Nowhere in the triplet state, is a vacant orbital available to facilitate nucleophile attack. In fact, the only species able to restore the low-spin ground state of the hexacoordinated products is the singlet square pyramidal ground state, via a vacant orbital on its empty coordination site. This association therefore presupposes triplet + singlet intersystem crossing in the five-coordinated fragment.*'[76]

Whilst the flattened state **2 ^{3}MC(F)** is energetically accessible, the steric clash between the two bpy ligands in **2** will prevent the coplanarisation of the Ru(bpy)$_2$ fragment, thereby inhibiting and precluding the

formation of a similar ^{3}MC(P)-like state. Indeed, crystallographically characterised bis(bipyridyl) complexes of the form *trans*-[Ru(bpy)$_2$(L)$_2$]$^{2+}$ (L = NH$_3$, py) are heavily distorted with a significant bending of the bpy ligands.[77, 78] Several attempts were made to locate a pseudo-pentacoordinate analogue of **2 ^{3}MC(F)** but initial guess geometries relaxed to either the **2 ^{3}MC(F)** or **2 ^{3}MC(B)** states. This signals the necessity of achieving approximate coplanarity of the Ru(N^N)(κ^2-btz) fragment in **3** and **4** to enable the formation of the observed *trans* photoproducts *via* the formally 16-electron pentacoordinate intermediates **3 ^{1}GS(P)** and **4 ^{1}GS(P)**.
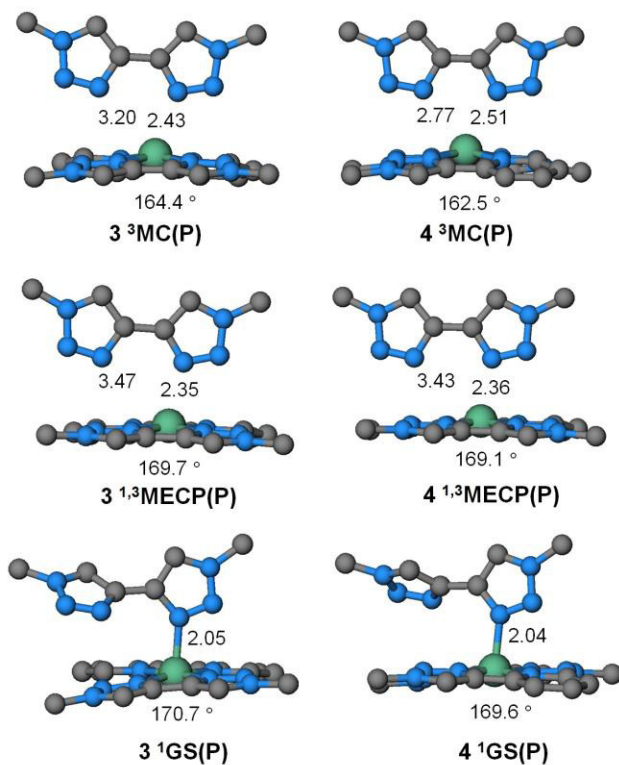

Figure 7. Relaxed geometries of ^{3}MC(P), ^{1,3}MECP(P) and ^{1}GS(P) states of **3** and **4** annotated with distances for elongated Ru-N bonds and the narrowest *trans* N-Ru-N angle θ of the approximate square planar base (hydrogen atoms omitted for clarity).

Triplet-triplet interconversions

Having characterised the ^{3}MLCT states and various classical ^{3}MC, flattened ^{3}MC(F) and pseudo-pentacoordinate ^{3}MC(P) states of **2** to **4,** we carried out nudged elastic band (NEB)[79, 80] calculations to determine energy barriers for their interconversions (Table 2 and Figures S8 to S10). This method is derived from Liotard's chain of states method[81, 82] and provides the minimum energy path connecting two points, without requiring

18

optimisation of the absolute transition state. It was found that for **2** conversion of the ^{3}MLCT state to any of the three ^{3}MC states **2 ^{3}MC(A/B/F)** proceeds with extremely low energy barriers of < 0.05 eV. Similarly, for **3**, all triplet-triplet interconversions involve very low energy barriers (Table 2). While these barriers are within the error expected for these calculations, what is evident is that these ^{3}PES are very flat and all states are readily accessible, and will be populated upon photoexcitation.

Regarding complex **4**, the least photoreactive of the complexes **2** to **4**, calculated interconversion barriers are larger but still relatively small, ranging from 0.10 to 0.25 eV. A shallow minimum is observed on the minimum energy NEB path from **3 ^{3}MLCT** to **3 ^{3}MC(P)** corresponding to the complex transiting through the **3 ^{3}MC(F)** region of the ^{3}PES as might be expected. Similar dips are observed in the NEB energy profiles for the transits from **3 ^{3}MC(B)** to **3 ^{3}MC(P)** and from **4 ^{3}MC(C)** to **4 ^{3}MC(P)**, the geometries at which correspond to distorted **3 ^{3}MC(F)** and **4 ^{3}MC(F)** states respectively.

Table 2. Calculated energy barriers (eV) from nudged elastic band calculations for triplet-triplet interconversions (quoted relative to state of origin). **A/B/C** stand for d_z^2-type 'classical' ^{3}MC states; **F** stands for new d_x^2-$_y^2$-type flattened ^{3}MC states; **P** stands for pseudo-pentacoordinate.

2 ^{3}MLCT→2 ^{3}MC(A)	0.05	**3 ^{3}MLCT→3 ^{3}MC(A)**	0.06	**4 ^{3}MC(A)→4 ^{3}MC(B)**	0.16
2 ^{3}MLCT→2 ^{3}MC(B)	0.01	**3 ^{3}MLCT→3 ^{3}MC(B)**	0.07	**4 ^{3}MC(A)→4 ^{3}MC(C)**	0.14
2 ^{3}MLCT→2 ^{3}MC(F)	0.01	**3 ^{3}MLCT→3 ^{3}MC(F)**	0.03	**4 ^{3}MC(B)→4 ^{3}MC(C)**	0.13
		3 ^{3}MLCT→3 ^{3}MC(P)	0.03	**4 ^{3}MC(A)→4 ^{3}MC(F)**	0.10
				4 ^{3}MC(B)→4 ^{3}MC(F)	0.10
2 ^{3}MC(A) →2 ^{3}MC(B)	0.07	**3 ^{3}MC(A)→3 ^{3}MC(B)**	0.15	**4 ^{3}MC(C)→4 ^{3}MC(F)**	0.25
2 ^{3}MC(A) →2 ^{3}MC(F)	0.13	**3 ^{3}MC(A)→3 ^{3}MC(F)**	0.05	**4 ^{3}MC(A)→4 ^{3}MC(P)**	0.23
2 ^{3}MC(B) →2 ^{3}MC(F)	0.06	**3 ^{3}MC(B)→3 ^{3}MC(F)**	0.06	**4 ^{3}MC(B)→4 ^{3}MC(P)**	0.21
		3 ^{3}MC(A)→3 ^{3}MC(P)	0.09	**4 ^{3}MC(C)→4 ^{3}MC(P)**	0.24
		3 ^{3}MC(B)→3 ^{3}MC(P)	0.08	**4 ^{3}MC(F)→4 ^{3}MC(P)**	0.13
		3 ^{3}MC(F)→3 ^{3}MC(P)	0.06		

Mechanistic insights and wider implications

Ruthenium tris(bidentate) complexes have been shown to undergo photochemically induced ligand loss, yielding either *cis* or *trans* photoproducts. Classical [3]MC states fail to explain the observed photoreactivity for *trans* photoproduct formation and we propose that this involves the new triplet and singlet states presented above. This discussion will focus on productive pathways, but given the low interconversion energy barriers, all triplet states can be populated. A depiction of the singlet and triplet excited state PES exemplified by **3** is shown in Figure 8.
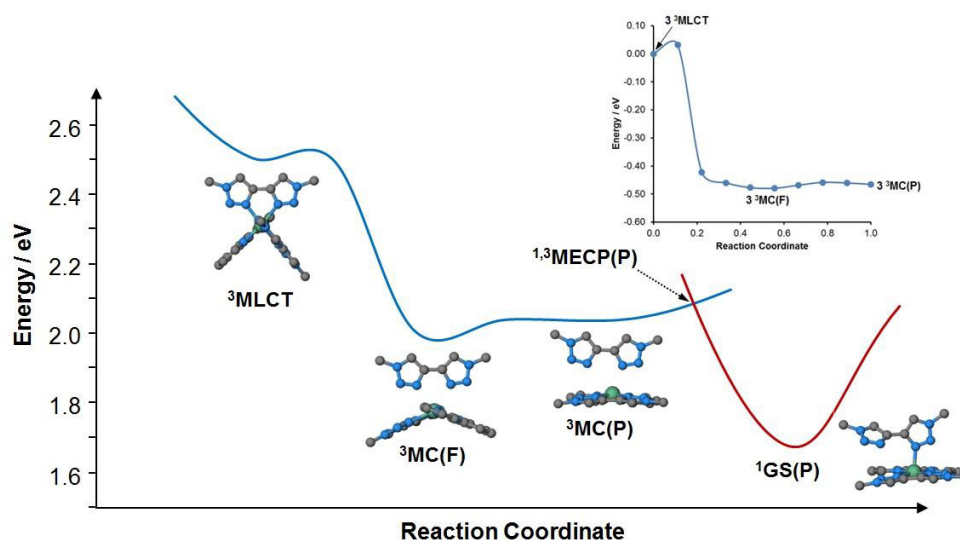

Figure 8. Schematic potential energy (quoted relative to the ground state of **3** being 0.0 eV) curve describing the structural evolution for **3**: Conversion of **3 [3]MLCT** to **3 [1]GS(P)** *via* **3 [3]MC(F)** and **3 [3]MC(P)**. Inset: Calculated NEB profile for the conversion of **3 [3]MLCT** to **3 [3]MC(P)** via **3 [3]MC(F)** (energy scale relative to **3 [3]MLCT** = 0 eV).

After initial excitation from the ground state for **3** yielding the [1]MLCT state, with subsequent intersystem crossing to the [3]MLCT state, we propose that this undergoes direct conversion to **3 [3]MC(F)** (blue line on Figure. 8), which is calculated to have a low energy barrier. This then undergoes conversion to the pseudo-square pyramidal pentacoordinate [3]MC state **3 [3]MC(P)**. **3 [3]MECP(P)** found to lie at only 0.05 eV above the minimum for this [3]MC state and, which is identified here for the first time, is therefore the only MECP

leading to photoproduct and is highly accessible. Optimisation of the singlet ground state starting from **3** **^{3}MECP(P)** results in formal κ^1-coordination of the distal btz ligand in the axial position of the square-pyramidal 16-electron species [Ru(bpy)(κ^2-btz)(κ^1-btz)]$^{2+}$ (**3 ^{1}GS(P)**, Figure 7, and red line on Figure 8). **3 ^{1}GS(P)** thus presents the appropriate singlet spin multiplicity and a free coordination site *trans* to the monodentate btz ligand available for rapid solvent coordination, in agreement with the observed monosolvento primary photoproduct **7**.[22]

In the case of **4**, after initial photoexcitation to a ^{1}MLCT state, rapid population of **4 ^{3}MC(A)** is likely to occur (blue line, Figure 9). Population of **4 ^{3}MC(F)** and **4 ^{3}MC(P)** states, 0.1 and 0.2 eV higher in energy than **4** **^{3}MC(A)** and transitioning to the ^{1}PES through **4 ^{1,3}MECP(P)**, will similarly yield the square pyramidal pentacoordinate 16-electron ground state species **4 ^{1}GS(P)** (red line, Figure 9) and precursor to the observed solvento species **8**. The relative slowness of conversion of **4** into **8** observed experimentally in NMR experiments was ascribed originally to the reduced overlap of its optical absorption spectrum with the emission profile of the lamp used for photolysis.[60] The theoretical data reveal that conversion of **4** to **8** might be additionally hampered relative to conversion of **3** to **7** due to the greater energy separation and greater energy barriers between **MC(A)** and **MECP(P)**.
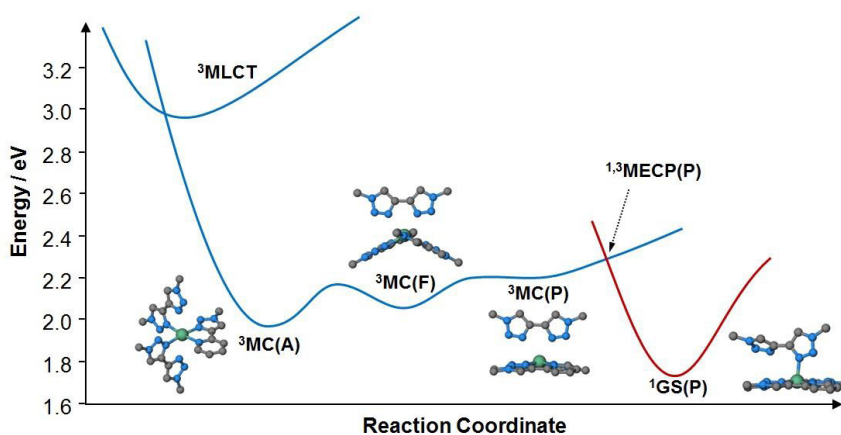

Figure 9. Schematic potential energy curve describing the structural evolution for **4**: Conversion of **4** ^{3}MC(A) to **4 ^{1}GS(P)** *via* **4 ^{3}MC(F)** and **4 ^{3}MC(P)**.

It must be pointed out that as all [3]MC states and [1,3]MECPs associated with them will be energetically accessible this will result in competing pathways after photoexcitation involving either restoration of the initial ground state or generation of solvated photoproduct *via* [3]MC(P) states. The relatively low experimentally determined quantum yield for photolysis of **4** would seem to underline this point.

To summarise, the observed *trans* photochemistry can be rationalized by the successive population of [3]MC(F) and [3]MC(P) species, which gives access to [1]GS(P) 16-electron intermediates prone to solvent trapping. On the other hand, the mechanism remains unclear regarding the formation of *cis* photoproducts. Classical MC states do not promote photochemistry, as indicated by the outcome of singlet state optimisation from the corresponding classical MECPs. Whilst the flattened state **2 [3]MC(F)** is energetically accessible and will be populated, the steric clash between the two bpy ligands in **2** will prevent the coplanarisation of the Ru(bpy)$_2$ fragment and inhibit the formation of a similar [3]MC(P)-like state subsequent and *trans* photoproduct. The inexistence of MC(P) states in bis(bpy) complexes may thus rationalize the absence of κ^1-ligand loss intermediates and *trans* photochemistry in this family of compounds. We propose that the photochemistry may well proceed through the [3]MC(F) state for **2** just as seems evident for **3** and **4**, but steric pressures or lack thereof determine the feasibility of a [3]MC(P)-like structure and hence the ultimate stereochemistry of the photoproducts.

In complexes **3** and **4** each of the two btz ligand plays a distinct role in the formation of a [1]GS(P) state and hence the final *trans* solvento photoproducts; the poor π-acceptor properties of the ligand enable it to readily occupy the distal position in the preceding [3]MC(F) state whilst the low steric demands enable the second btz ligand to become co-planar with the third (bpy or pytz) chelate ligand in the [3]MC(P) state. Whilst in retrospect the existence of [3]MC(F) and [3]MC(P) states is thus readily apparent from the observed *trans* stereochemistry for the photoproducts of **3** and **4** we strongly believe that [3]MC(F)-type states are far from unique to the systems described here. Firstly, the discovery of a [3]MC(F) minimum for **2** with a low energy barrier for its population from the [3]MLCT state clearly demonstrates that such states could be highly accessible in the large number of known photochemically reactive systems in which the Ru(bpy)$_2$ moiety is ubiquitous. Indeed, we have noted the existence of such a [3]MC(F) state in the photorearrangement mechanism of a Ru(bpy)$_2$-containing chelated sulphoxide complex.[20] In systems where the ultimate photoproduct stereochemistry exhibits retention of the *cis*

arrangement of the reactants the involvement of such ^{3}MC(F) may not be immediately apparent but such states may be crucial to the mechanism of many processes. Great advances have been made in the past few years in the theoretical, and indeed experimental characterisation of (classical) ^{3}MC states. However, it is possible that this very retention of stereochemistry is the main reason that the novel ^{3}MC(F)-type states highlighted here have been, not-so-much overlooked, but unanticipated in previous studies. Work is continuing in our groups to establish the mechanism for formation of *cis* photoproducts from the ^{3}MC state manifold and will be reported elsewhere in due course.

A common route to promote ligand ejection reactivity in ruthenium(II) tris(bidentate) complexes involves the incorporation of steric congestion to weaken Ru-N bonds and stabilise ^{3}MC states thereby promoting their population, provided the ^{3}MLCT and ^{3}MC PES are not nested.[83] The results presented here, involving the incorporation of sterically unencumbered triazole-containing ligands with poor π-acceptor character displaying original ^{3}PES topologies, therefore offer new insights into alternative design strategies for complexes that exhibit photochemical ligand ejection or photomechanical motion. The photoejection of a btz ligand has been reported for the complex [Ir(dfptz)$_2$(btz)]$^{2+}$ (dfptzH = 4-(2,4-difluorophenyl)-1,2,3-triazole).[56] Based on the results presented here for **2** and the known propensity of the [Ir(C^N)$_2$] fragments to flatten in ^{3}MC states of triscyclometalated iridium(III) complexes[73] it is therefore possible that a ^{3}MC(F)-type state is also operative in this system. As we have alluded to before, a flattened ^{3}MC state was shown to be a crucial intermediate state in the photoisomerisation of a [Ru(bpy)$_2$]-containing chelating sulphoxide complex.[20] It is possible that such flattened states play a crucial role in the photorelease mechanism of other ligands lacking in π-acceptor character including diamines and dithioether type ligands[84] investigated recently but may also be intimately involved in the formation of photodechelation products proposed previously for [Ru(bpy)$_3$]$^{2+}$ type complexes.[85] Excited state dynamics involving photomechanical ligand motion may also be involved in light induced spin crossover complexes.[86] Whilst the ligand systems reported here have facilitated the illumination of these new and original flattened ^{3}MC states they may have as yet unrecognised impact and relevance in a wider range of metal complex systems exhibiting light induced phenomena.

Conclusions

Tris(bidentate) ruthenium(II) complexes may undergo photochemical ligand loss yielding either *cis* or *trans* photoproducts. This work has focused on the case of two bis(btz) complexes which produce exclusively *trans* photoproducts. We have identified and characterised highly novel ^{3}MC states (flattened and pentacoordinate), which we propose are major actors in the mechanism of formation of *trans* photoproducts but reveal the ease with which the flattened ^{3}MC can be populated in a mono(btz) complex where only a *cis* photoproduct is observed. The ^{3}MC region is a vast basin, which is favourable to photochemistry from the point of view of entropic factors. Experimental characterisation of such a landscape is certainly an extreme challenge, however, computational approaches can offer significant insights. 'Classical' ^{3}MC states in these systems cannot account for the mechanism of photoreactivity. The novel states proposed here fill the gap in our knowledge and represent the missing link in the photoreactive mechanism. Having identified a pentacoordinate singlet/triplet crossing point, and describing for the first time 16-electron singlet closed shell pentacoordinate ligand dechelation intermediates, this enables us to propose a full mechanism for solvent coordination that obeys Wigner's rules. Knowledge of the origin and nature of ^{3}MC states of the type described here and their corresponding MECPs is compulsory when attempting to rationalise the mechanism of photochemical ligand rearrangements and dissociation reactions for transition metal complex systems. With the mechanism forming *trans* photoproducts having been elucidated work is currently in progress in our laboratories to complete the mechanism for the formation of *cis* photoproducts and demonstrate the wider significance and impact of such flattened ^{3}MC states in transition metal photochemistry.

Supporting Information

Mulliken spin density plots for triplet states, plots of frontier molecular orbitals, results from relaxed potential energy surface scans and nudged elastic band calculations, summarised structural data for triplet states and calculated atomic coordinates for optimised singlet and triplet minima and minimum energy singlet-triplet crossing points.

Acknowledgements

Computational Details

The singlet ground state geometries of the complexes were optimised at the B3LYP level of theory (20 % Hartree-Fock)[87] in the gas phase using the NWChem 6.3 software package.[88] Molecular structures and molecular orbital plots were visualised using the ECCE software package. The Stuttgart-Dresden relativistic small-core ECP[89] and associated basis set were used for ruthenium and 6-311G* basis sets[90] were used for all other atoms. The lowest lying ^{3}MLCT states for complexes **1** to **3** were calculated starting from the singlet ground state geometries and using the constraint of a spin multiplicity of 3 (UDFT). In the case of **5** where the lowest lying triplet state is ^{3}MC in character, the D_3 symmetric ^{3}MLCT state was optimised imposing D_3 symmetry. To calculate optimised geometries of classical Jahn-Teller type ^{3}MC states the distribution of the ground state dσ* orbitals were examined and the bond lengths for each Ru-N bond participating in these orbitals was manually elongated to generate an initial estimate geometry. These were then allowed to optimise under the constraint of a spin multiplicity of 3. To confirm that minima had been obtained in geometry optimisations vibration frequency calculations were carried out. In some cases small negative vibrational modes were observed (< -50 cm^{-1}) and are characterised by the rotation of the methyl groups of the btz ligands. Optimisation of the **3 ^{3}MC(F)'** minimum bearing a distal bpy ligand was achieved at the same level of theory using Orca 3.0 (Cite orca here) starting from a favourable guess geometry (Ru-bpy bonds set to 2.5 Å and θ angle set to 160°) using a reduced

stepsize (maxstep 0.1). Triplet state potential energy surface scans were carried out by iteratively elongating/shortening the desired Ru-N bond distances in 0.02 Å steps. At each step the complexes were optimised with the Ru-N bond length in question held constant. Molecular orbital vectors from the previous geometry iteration were discarded at each step and reformulated afresh. The evolution of the molecular geometries during the progress of the PES scans were animated using the JMol software package.

The minimum energy paths (MEPs) on the ^{3}PES were optimized using the nudged elastic band (NEB) method[79, 80] using NWChem 6.6. The geometries were prepared (oriented and superimposed) using lab-developed programs to minimize the discrepancy between start and end geometries. A 10-bead initial path, created by IDPP interpolation[91] using the IDPP_ase program (https://wiki.fysik.dtu.dk/ase/tutorials/neb/idpp.html), was provided for the NEB calculation. The NEB calculation itself was performed using the same functional, pseudo potential and basis sets as for minima optimisation. The following parameters were used for the NEB calculations: algorithm 0, kbeads 0.05, stepsize 0.2, nbeads 10. Two NEB calculations were run sequentially using two different SCF convergers : for the first 10 iterations the wavefunction was converged with DIIS; then at least 20 iterations were run using the semiquadratic CGMIN converger (setting the convergence gradient to $5e^{-5}$) to ensure convergence on the lowest electronic triplet excited state. Out of the 26 NEB calculations, three of them displayed abnormally abrupt profiles and were restarted using an increased number of beads (20 in this case), as proposed in the NWChem manual (**2 ^{3}MLCT-2 ^{3}MC(A)**; **3 ^{3}MLCT-3 ^{3}MC(A)**; **3 ^{3}MLCT-^{3} 3MC(B)**). In addition, the barriers from **4 ^{3}MC(A)**, **4 ^{3}MC(B)** and **4 ^{3}MC(C)** to **4 ^{3}MC(F)** were obtained from NEB calculations started from **4 ^{3}MC(F)**.

^{3}MC/^{1}GS minimum energy crossing points (MECPs) were optimized starting from the relevant (NWChem) ^{3}MC geometries using Orca 3.0[92] under similar conditions (B3LYP functional, same Stuttgart-Dresden pseudopotential on Ru, def2-TZVP basis set[93] and def2-TZVP/j auxiliary basis set[94] on Ru, and 6-311G* basis sets on all other atoms). Convergence of the wavefunction was also achieved using DIIS followed by a semiquadratic converger (here SOSCF). Frequency calculations were run on the MECP geometries using the specific SurfCrossNumFreq keyword. Triplet state singly occupied natural orbitals were plotted from Orca single point calculations with 0.04 isovalue using Gabedit.[95]

References

1.   A. Juris, V. Balzani, F. Barigelletti, S. Campagna, P. Belser and A. Vonzelewsky, *Coord. Chem. Rev.*, 1988, **84**, 85-277.

2.   V. Balzani, P. Ceroni and A. Juris, *Photochemistry and Photophysics: Concepts, Research, Applications*, Wiley-VCH, 2014.

3.   D. G. Brown, N. Sanguantrakun, B. Schulze, U. S. Schubert and C. P. Berlinguette, *J. Am. Chem. Soc.*, 2012, **134**, 12354-12357.

4.   S. Lamansky, P. Djurovich, D. Murphy, F. Abdel-Razzaq, H.-E. Lee, C. Adachi, P. E. Burrows, S. R. Forrest and M. E. Thompson, *J. Am. Chem. Soc.*, 2001, **123**, 4304-4312.

5.   E. Quartapelle Procopio, M. Mauro, M. Panigati, D. Donghi, P. Mercandelli, A. Sironi, G. D'Alfonso and L. De Cola, *J. Am. Chem. Soc.*, 2010, **132**, 14397-14399.

6.   Q. Sun, B. Dereka, E. Vauthey, L. M. Lawson Daku and A. Hauser, *Chem. Sci.*, 2016, **8**, 223-230.

7.   Q. Sun, S. Mosquera-Vazquez, Y. Suffren, J. Hankache, N. Amstutz, L. M. L. Daku, E. Vauthey and A. Hauser, *Coord. Chem. Rev.*, 2015, **282-283**, 87-99.

8.   M. Abrahamsson, M. Jäger, R. J. Kumar, T. Österman, P. Persson, H.-C. Becker, O. Johansson and L. Hammarström, *J. Am. Chem. Soc.*, 2008, **130**, 15533-15542.

9.   T. Sajoto, P. I. Djurovich, A. B. Tamayo, J. Oxgaard, W. A. Goddard and M. E. Thompson, *J. Am. Chem. Soc.*, 2009, **131**, 9813-9822.

10.   Y. Sun, Y. Liu and C. Turro, *J. Am. Chem. Soc.*, 2010, **132**, 5594-5595.

11.   C. Kreitner and K. Heinze, *Dalton Trans.*, 2016, **45**, 13631-13647.

12.   A. Soupart, I. M. Dixon, F. Alary and J.-L. Heully, *Submitted Manuscript*, 2017.

13.   S. G. Shepard, S. M. Fatur, A. K. Rappé and N. H. Damrauer, *J. Am. Chem. Soc.*, 2016, **138**, 2949-2952.

14.   S. M. Fatur, S. G. Shepard, R. F. Higgins, M. P. Shores and N. H. Damrauer, *J. Am. Chem. Soc.*, 2017, **139**, 4493-4505.

15.   L. L. Jamula, A. M. Brown, D. Guo and J. K. McCusker, *Inorg. Chem.*, 2014, **53**, 15-17.

16.   J. Nance, D. N. Bowman, S. Mukherjee, C. T. Kelley and E. Jakubikova, *Inorg. Chem.*, 2015, **54**, 11259-11268.

17.   S. Zerdane, L. Wilbraham, M. Cammarata, O. Iasco, E. Riviere, M. L. Boillot, I. Ciofini and E. Collet, *Chem. Sci.*, 2017.

18.   M. Reinhard, G. Auböck, N. A. Besley, I. P. Clark, G. M. Greetham, M. W. D. Hanson-Heine, R. Horvath, T. M. Murphy, T. J. Penfold, M. Towrie, M. W. George and M. Chergui, *J. Am. Chem. Soc.*, 2017, **139**, 7335-7347.

19.   B. Durham, J. V. Caspar, J. K. Nagle and T. J. Meyer, *J. Am. Chem. Soc.*, 1982, **104**, 4803-4810.

20.   A. J. Göttle, I. M. Dixon, F. Alary, J. L. Heully and M. Boggio-Pasqua, *J. Am. Chem. Soc.*, 2011, **133**, 9172-9174.

21.   B. S. Howerton, D. K. Heidary and E. C. Glazer, *J. Am. Chem. Soc.*, 2012, **134**, 8324-8327.

22.   Y. Liu, D. B. Turner, T. N. Singh, A. M. Angeles-Boza, A. Chouai, K. R. Dunbar and C. Turro, *J. Am. Chem. Soc.*, 2009, **131**, 26-27.

23.   B. A. McClure, E. R. Abrams and J. J. Rack, *J. Am. Chem. Soc.*, 2010, **132**, 5428-5436.

24.   M. A. Sgambellone, A. David, R. N. Garner, K. R. Dunbar and C. Turro, *Journal of the American Chemical Society*, 2013, **135**, 11274-11282.

25.   E. Baranoff, J. P. Collin, J. Furusho, Y. Furusho, A. C. Laemmel and J. P. Sauvage, *Inorg. Chem.*, 2002, **41**, 1215-1222.

26.   J. P. Collin, D. Jouvenot, M. Koizumi and J. P. Sauvage, *Inorg. Chem.*, 2005, **44**, 4693-4698.

27.   S. Fanni, F. M. Weldon, L. Hammarstrom, E. Mukhtar, W. R. Browne, T. E. Keyes and J. G. Vos, *Eur. J. Inorg. Chem.*, 2001, 529-534.

28.   T. N. Singh and C. Turro, *Inorg. Chem.*, 2004, **43**, 7260-7262.

29.   M. R. Camilo, C. R. Cardoso, R. M. Carlos and A. B. P. Lever, *Inorg. Chem.*, 2014, **53**, 3694-3708.

30.   L. Ding, L. W. Chung and K. Morokuma, *Journal of Chemical Theory and Computation*, 2014, **10**, 668-675.

31.   A. J. Göttle, F. Alary, I. M. Dixon, J. L. Heully and M. Boggio-Pasqua, *Inorg. Chem.*, 2014, **53**, 6752-6760.

32.   L. Salassa, C. Garino, G. Salassa, R. Gobetto and C. Nervi, *J. Am. Chem. Soc.*, 2008, **130**, 9590-9597.

33.   Y. J. Tu, S. Mazumder, J. F. Endicott, C. Turro, J. J. Kodanko and H. B. Schlegel, *Inorg. Chem.*, 2015, **54**, 8003-8011.

34.   J. K. White, R. H. Schmehl and C. Turro, *Inorg. Chim. Acta*, 2017, **454**, 7-20.

35.   S. J. Carrington, I. Chakraborty and P. K. Mascharak, *Chem. Commun.*, 2013, **49**, 11254-11256.

36.   H. Li, L. Zhang, L. Zheng, X. Li, X. Fan and Y. Zhao, *Chem. Eur. J.*, 2016, **22**, 14285-14292.

37.   J. D. Knoll, B. A. Albani, C. B. Durr and C. Turro, *J. Phys. Chem. A*, 2014, **118**, 10603-10610.

38.   J. D. Knoll, B. A. Albani and C. Turro, *Acc. Chem. Res.*, 2015, **48**, 2280-2287.

39.   W. K. C. Lo, G. S. Huff, J. R. Cubanski, A. D. W. Kennedy, C. J. McAdam, D. A. McMorran, K. C. Gordon and J. D. Crowley, *Inorg. Chem.*, 2015, **54**, 1572-1587.

40.   F. Weisser, S. Plebst, S. Hohloch, M. Van Der Meer, S. Manck, F. Führer, V. Radtke, D. Leichnitz and B. Sarkar, *Inorg. Chem.*, 2015, **54**, 4621-4635.

41.   J. D. Knoll and C. Turro, *Coord. Chem. Rev.*, 2015, **282-283**, 110-126.

42.   F. Alary, J. L. Heully, L. Bijeire and P. Vicendo, *Inorg. Chem.*, 2007, **46**, 3154-3165.

43.   F. Alary, M. Boggio-Pasqua, J.-L. Heully, C. J. Marsden and P. Vicendo, *Inorg. Chem.*, 2008, **47**, 5259-5266.

44.   Q. Sun, S. Mosquera-Vazquez, L. M. L. Daku, L. Guénée, H. A. Goodwin, E. Vauthey and A. Hauser, *J. Am. Chem. Soc.*, 2013, **135**, 13660−13663.

45.   J. D. Crowley and D. A. McMorran, *Top. Heterocycl. Chem.*, 2012, **28**, 31-83.

46.   P. I. P. Elliott, *SPR Organometallic Chemistry: Volume 39*, 2014, **39**, 1.

47.   J. M. Fernández-Hernández, C.-H. Yang, J. I. Beltrán, V. Lemaur, F. Polo, R. Fröhlich, J. Cornil and L. De Cola, *J. Am. Chem. Soc.*, 2011, **133**, 10543-10558.

48.   M. Mydlak, C. Bizzarri, D. Hartmann, W. Sarfert, G. Schmid and L. De Cola, *Adv. Funct. Mater.*, 2010, **20**, 1812-1820.

49.   E. Orselli, R. Q. Albuquerque, P. M. Fransen, R. Froehlich, H. M. Janssen and L. De Cola, *J. Mater. Chem.*, 2008, **18**, 4579-4590.

50.   S. Zanarini, M. Felici, G. Valenti, M. Marcaccio, L. Prodi, S. Bonacchi, P. Contreras-Carballada, R. M. Williams, M. C. Feiters, R. J. M. Nolte, L. De Cola and F. Paolucci, *Chem. Eur. J.*, 2011, **17**, 4640-4647.

51.   B. Beyer, C. Ulbricht, D. Escudero, C. Friebe, A. Winter, L. Gonzalez and U. S. Schubert, *Organometallics*, 2009, **28**, 5478.

52.   S. Ladouceur, D. Fortin and E. Zysman-Colman, *Inorg. Chem.*, 2011, **50**, 11514-11526.

53.   K. N. Swanick, S. Ladouceur, E. Zysman-Colman and Z. Ding, *Chem. Commun.*, 2012, **48**, 3179-3181.

54.   K. N. Swanick, S. Ladouceur, E. Zysman-Colman and Z. Ding, *Angew. Chem. Int. Ed.*, 2012, **51**, 11079-11082.

55.   I. Stengel, A. Mishra, N. Pootrakulchote, S. J. Moon, S. M. Zakeeruddin, M. Grätzel and P. Bäuerle, *J. Mater. Chem.*, 2011, **21**, 3726-3734.

56.   L. Donato, P. Abel and E. Zysman-Colman, *Dalton Trans.*, 2013, **42**, 8402-8412.

57.   J. T. Fletcher, B. J. Bumgarner, N. D. Engels and D. A. Skoglund, *Organometallics*, 2008, **27**, 5430-5433.

58. U. Monkowius, S. Ritter, B. König, M. Zabel and H. Yersin, *Eur. J. Inorg. Chem.*, 2007, **2007**, 4597-4606.

59. D. A. Ross, P. A. Scattergood, A. Babaei, A. Pertegás, H. J. Bolink and P. I. P. Elliott, *Dalton Trans.*, 2016.

60. P. A. Scattergood, U. Khushnood, A. Tariq, D. J. Cooke, C. R. Rice and P. I. P. Elliott, *Inorg. Chem.*, 2016, **55**, 7787-7796.

61. C. E. Welby, G. K. Armitage, H. Bartley, A. Sinopoli, B. S. Uppal and P. I. P. Elliott, *Photochem.Photobiol. Sci.*, 2014, **13**, 735-738.

62. C. E. Welby, G. K. Armitage, H. Bartley, A. Wilkinson, A. Sinopoli, B. S. Uppal, C. R. Rice and P. I. P. Elliott, *Chem. Eur. J.*, 2014, **20**, 8467-8476.

63. C. E. Welby, C. R. Rice and P. I. P. Elliott, *Angew. Chem. Int. Ed.*, 2013, **52**, 10826–10829.

64. A. Mattiuzzi, I. Jabin, C. Moucheron and A. Kirsch-De Mesmaeker, *Dalton Trans.*, 2011, **40**, 7395-7402.

65. P. A. Scattergood, D. A. W. Ross, C. R. Rice and P. I. P. Elliott, *Angew. Chem. Int. Ed.*, 2016, **55**, 10697-10701.

66. C. E. Welby, S. Grkinic, A. Zahid, B. S. Uppal, E. A. Gibson, C. R. Rice and P. I. P. Elliott, *Dalton Trans.*, 2012, **41**, 7637-7646.

67. S. E. Greenough, G. M. Roberts, N. A. Smith, M. D. Horbury, R. G. McKinlay, J. M. Zurek, M. J. Paterson, P. J. Sadler and V. G. Stavros, *PCCP*, 2014, **16**, 19141-19155.

68. A. Li, J. K. White, K. Arora, M. K. Herroon, P. D. Martin, H. B. Schlegel, I. Podgorski, C. Turro and J. J. Kodanko, *Inorg. Chem.*, 2016, **55**, 10−12.

69. L. Salassa, C. Garino, G. Salassa, C. Nervi, R. Gobetto, C. Lamberti, D. Gianolio, R. Bizzarri and P. J. Sadler, *Inorg. Chem.*, 2009, **48**, 1469-1481.

70. A. J. Göttle, F. Alary, M. Boggio-Pasqua, I. M. Dixon, J. L. Heully, A. Bahreman, S. H. C. Askes and S. Bonnet, *Inorg. Chem.*, 2016, **55**, 4448-4456.

71. N. Planas, L. Vigara, C. Cady, P. Miró, P. Huang, L. Hammarström, S. Styring, N. Leidel, H. Dau, M. Haumann, L. Gagliardi, C. J. Cramer and A. Llobet, *Inorg. Chem.*, 2011, **50**, 11134-11142.

72. X. Zhou, P. L. Burn and B. J. Powell, *Inorganic Chemistry*, 2016, **55**, 5266-5273.

73. G. Treboux, J. Mizukami, M. Yabe and S. Nakamura, *Chem. Lett.*, 2007, **36**, 1344-1345.

74. J. N. Harvey, *Wiley Interdisciplinary Reviews: Computational Molecular Science*, 2014, **4**, 1-14.

75. R. Poli and J. N. Harvey, *Chem. Soc. Rev.*, 2003, **32**, 1-8.

76. L. G. Vanquickenborne and A. Ceulemans, *Coord. Chem. Rev.*, 1983, **48**, 157-202.

77. P. Bonneson, J. L. Walsh, W. T. Pennington, A. W. Cordes and B. Durham, *Inorg. Chem.*, 1983, **22**, 1761-1765.

78. A. W. Cordes, B. Durham, W. T. Pennington, B. Kuntz and L. Allen, *Journal of Crystallographic and Spectroscopic Research*, 1992, **22**, 699-704.

79. G. Henkelman, G. Jóhannesson and H. Jónsson, in *Theoretical Methods in Condensed Phase Chemistry*, ed. S. D. Schwartz, Kluwer Academic, 2000, pp. 269–300.

80. H. Jonsson, G. Mills and K. W. Jacobsen, in *Classical and Quantum Dynamics in Condensed Phase Simulations*, eds. B. J. Berne, G. Cicotti and D. F. Coker, World Scientific, 1998, pp. 385–404.

81. D. Liotard, *Int. J. Quantum Chem*, 1992, **44**, 723-741.

82. D. Liotard and J.-P. Penot, in *Numerical methods in the study of critical phenomena*, eds. J. Della Dora, J. Demongeot and B. Lacolle, Springer, 1981, pp. 213-221.

83. P. J. Vallett and N. H. Damrauer, *J. Phys. Chem. A*, 2013, **117**, 6489-6507.

84. R. N. Garner, L. E. Joyce and C. Turro, *Inorg. Chem.*, 2011, **50**, 4384-4391.

85. D. W. Thompson, J. F. Wishart, B. S. Brunschwig and N. Sutin, *J. Phys. Chem. A*, 2001, **105**, 8117-8122.

86. Y. Jiang, L. C. Liu, H. M. Müller-Werkmeister, C. Lu, D. Zhang, R. L. Field, A. Sarracini, G. Moriena, E. Collet and R. J. D. Miller, *Angew. Chem. Int. Ed.*, 2017, **56**, 7130-7134.

87. P. J. Stephens, F. J. Devlin, C. F. Chabalowski and M. J. Frisch, *J. Phys. Chem.*, 1994, **98**, 11623-11627.

88. M. Valiev, E. J. Bylaska, N. Govind, K. Kowalski, T. P. Straatsma, H. J. J. van Dam, D. Wang, J. Nieplocha, E. Apra, T. L. Windus and W. A. de Jong, *Comput. Phys. Commun.*, 2010, **181**, 1477.

89. D. Andrae, U. Haussermann, M. Dolg, H. Stoll and H. Preuss, *Theoretica Chimica Acta*, 1990, **77**, 123-141.

90. R. Krishnan, J. S. Binkley, R. Seeger and J. A. Pople, *J. Chem. Phys.*, 1980, **72**, 650-654.

91. S. Smidstrup, A. Pedersen, K. Stokbro and H. Jónsson, *J. Chem. Phys.*, 2014, **140**.

92. F. Neese, *Wiley Interdisciplinary Reviews: Computational Molecular Science*, 2012, **2**, 73-78.

93. F. Weigend and R. Ahlrichs, *PCCP*, 2005, **7**, 3297-3305.

94. F. Weigend, *PCCP*, 2006, **8**, 1057-1065.

95. A. R. Allouche, *J. Comput. Chem.*, 2011, **32**, 174-182.